

AD-A190 899

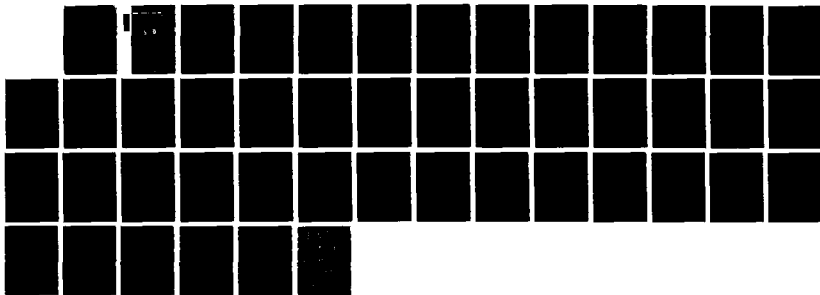
ENHANCED CHANNEL TRACKING DUE TO BEAM-GENERATED
MAGNETIC FIELDS(U) MISSION RESEARCH CORP ALBUQUERQUE NM
D R WELCH ET AL. 10 JUN 86 AMRC-R-814 N60921-85-C-0044

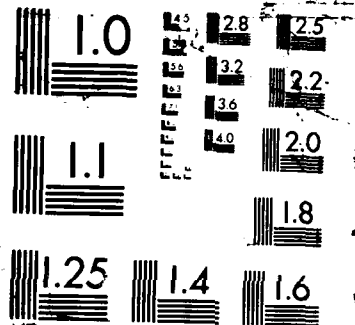
1/1

UNCLASSIFIED

F/G 20/8

NL





4

Mission Research Corporation

DTIC FILE COPY

ENHANCED CHANNEL TRACKING DUE TO BEAM-GENERATED
MAGNETIC FIELDS

D. R. Welch
B. B. Godfrey

DTIC
ELECTE
JAN 22 1988
S D

June 1986

Prepared for: SCIENCE APPLICATIONS INTERNATIONAL CORPORATION
5150 El Camino Real
Suite B-31
Los Altos, CA 94022

Under: Subcontract SAIC 15-860022-79
Prime Contract N60921-85-C-0044

Prepared by: MISSION RESEARCH CORPORATION
1720 Randolph Road, SE.
Albuquerque, NM 87106

APPROVED FOR PUBLIC RELEASE; DISTRIBUTION IS UNLIMITED.

88 1 13 021

UNCLASSIFIED
SECURITY CLASSIFICATION OF THIS PAGE

A190 899


1a REPORT SECURITY CLASSIFICATION UNCLASSIFIED		1b RESTRICTIVE MARKINGS	
2a SECURITY CLASSIFICATION AUTHORITY		3 DISTRIBUTION/AVAILABILITY OF REPORT Approved for public release; distribution is unlimited.	
2b DECLASSIFICATION/DOWNGRADING SCHEDULE		5. MONITORING ORGANIZATION REPORT NUMBER(S)	
4 PERFORMING ORGANIZATION REPORT NUMBER(S) AMRC-R-814		7a. NAME OF MONITORING ORGANIZATION	
6a NAME OF PERFORMING ORGANIZATION Mission Research Corporation		6b OFFICE SYMBOL (if applicable) AMRC	
6c ADDRESS (City, State, and ZIP Code) 1720 Randolph Road, S.E. Albuquerque, New Mexico 87106		7b. ADDRESS (City, State, and ZIP Code)	
8a. NAME OF FUNDING/SPONSORING ORGANIZATION Naval Surface Weapons Center		8b OFFICE SYMBOL (if applicable)	
8c ADDRESS (City, State, and ZIP Code) 10901 New Hampshire Avenue White Oak Silver Spring, Maryland 20903-5000		9 PROCUREMENT INSTRUMENT IDENTIFICATION NUMBER	
10 SOURCE OF FUNDING NUMBERS		PROGRAM ELEMENT NO	
PROJECT NO		TASK NO	
WORK UNIT ACCESSION NO		11 TITLE (Include Security Classification) ENHANCED CHANNEL TRACKING DUE TO BEAM-GENERATED MAGNETIC FIELDS	
12 PERSONAL AUTHOR(S) D. R. Welch and B. B. Godfrey		13a TYPE OF REPORT	
13b TIME COVERED FROM TO		14 DATE OF REPORT (Year, Month, Day) 1986 June 10	
15 PAGE COUNT 39		16 SUPPLEMENTARY NOTATION	
17 COSATI CODES		18 SUBJECT TERMS (Continue on reverse if necessary and identify by block number)	
FIELD		GROUP	
SUB-GROUP			
19 ABSTRACT (Continue on reverse if necessary and identify by block number)		The complete frozen-field Maxwell equations are used to study the tracking behavior of an electron beam in a channel. The three types of channels considered contain conductivity, reduced density or a combination of both. The analytic work includes the derivation of the tracking force for a beam propagating entirely inside a square conductivity channel. The resulting expression reduces to E. Lee's electrostatic expression in the limit of small conductivity. However, for finite conductivity, magnetic tracking is dominant near the head of the beam, particularly for short rise-time beams.	
The numerical work using the three-dimensional simulation code IPROP shows high values for channel tracking with large optimal initial conductivities (roughly 1×10^{10} scalar conductivity). For all three types of channels, tracking forces of 20 gauss are calculated for fast-rise 10-kA pencil beams in a 1-cm channel. Trumpet-shaped beams require larger channel radii to produce significant tracking. Forces of approximately 5 gauss are calculated for a			
20 DISTRIBUTION/AVAILABILITY OF ABSTRACT <input type="checkbox"/> UNCLASSIFIED/UNLIMITED <input type="checkbox"/> SAME AS RPT <input type="checkbox"/> DTIC USERS		21 ABSTRACT SECURITY CLASSIFICATION Unclassified	
22a NAME OF RESPONSIBLE INDIVIDUAL		22b TELEPHONE (Include Area Code)	
		22c OFFICE SYMBOL	

UNCLASSIFIED

SECURITY CLASSIFICATION OF THIS PAGE

Block 19 concluded.

5-cm offset channel with 3-cm radius. This work suggests tracking forces may be an order of magnitude greater than previously thought.

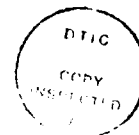


UNCLASSIFIED

SECURITY CLASSIFICATION OF THIS PAGE

CONTENTS

<u>Chapter</u>		<u>Page</u>
1	INTRODUCTION	1
2	ANALYTICAL MODELS	4
	A. FROZEN-FIELD EQUATIONS	4
	B. DERIVATION OF THE TRACKING FORCE	6
	C. RESULTS	9
3	NUMERICAL SIMULATIONS	19
	A. PENCIL BEAM	20
	B. TRUMPET BEAM	29
4	DISCUSSION	34
5	CONCLUSIONS	37
	REFERENCES	39



Accession For	
NTIS CRA&I	<input checked="" type="checkbox"/>
DTIC TAB	<input type="checkbox"/>
Unannounced	<input type="checkbox"/>
Justification	
By	
On (Date)	
Availability Code	
Dist	Availability Code
A-1	

ILLUSTRATIONS

<u>Figure</u>		<u>Page</u>
1	The total tracking force with the electric and magnetic components, calculated for an electron beam using the analytic model, are plotted versus the beam coordinate, τ . The 10-kA beam with a 0.25-cm displacement propagates through a 1-cm radius channel with 0.2-cm^{-1} conductivity.	12
2	The tracking force, on a 10-kA beam with a 15-cm rise time in a 1-cm channel with $\sigma = 0.5\text{ cm}^{-1}$, is plotted using the results from the analytic model and IPROP. In (a), the total force is given and, in (b), the electric and magnetic components of the force are plotted. Note the good agreement when the forces are relatively large.	13
3	The tracking force on a 10-kA beam with a 0.25-cm displacement is calculated using the analytic model with $X = 1, 2$ and 4 and compared with Lee's expression. The 1-cm channel has $\sigma = 1\text{ cm}^{-1}$. The drift-tube radii are 2.7, 7.4 and 55, corresponding to $X = 1, 2$ and 4 , respectively.	16
4	The maximum tracking force on a 10-kA beam in a 1-cm channel with $\sigma = 0.2\text{ cm}^{-1}$ is plotted for variable beam rise time.	17
5	The tracking force, calculated using IPROP, is sketched versus τ . The channels considered are conductivity, density and combination (conductivity/density). The 10-kA, 50-MeV beam has a 0.5-cm radius with a Bennett profile. The Gaussian-shaped channel has $r_c = 1\text{ cm}$.	21
6	The electric and magnetic components of the total tracking force are plotted for a 10-kA beam with a 15-ns rise time in a 1-cm conductivity channel.	23
7	The electric and magnetic components of the total tracking force are plotted for a 10-kA beam with a 15-ns rise time in a 1-cm density channel.	24
8	The electric and magnetic components of the total tracking force are plotted for a 10-kA beam with a 120-ns rise time in a 1-cm density channel.	25
9	The tracking behavior of a trumpet beam and a 2-cm radius pencil beam is compared. The 3-cm conductivity channel was offset 0.75 cm. The trumpet shape is given by Eq. 33.	30

ILLUSTRATIONS (Concluded)

<u>Figure</u>		<u>Page</u>
10	The tracking forces for a trumpet beam in a density channel is plotted. The 3-cm radius channel had a 0.1-atm on-axis density.	32

TABLES

<u>Table</u>		<u>Page</u>
1	Optimization of channel tracking in conductivity channel	26
2	Optimization of tracking in density channel	28
3	Optimization of tracking in density/conductivity channel	28
4	Trumpet beam tracking in conductivity channel	31

CHAPTER 1

INTRODUCTION

In this paper, we will study the response of an intense relativistic electron beam to a preformed channel. The channel, which may have initial conductivity, depressed density or both, could be produced by an initial charged-particle beam, laser or electrical discharge. If a beam is introduced displaced from the channel axis and through its own interaction with the channel is forced towards the axis, the beam is said to "track". Maxwell's complete equations will be used in analytic and numerical work to study channel tracking in detail.

The new analytic work presented in this paper builds upon the electrostatic tracking model of Lee.¹ Lee first developed an analytic tracking model for a beam propagating entirely inside a square conductivity channel. He showed that, in the limit of small conductivity, the problem becomes purely electrostatic. In order to take into account the magnetic effects associated with more sizable conductivity, we used the full frozen-field equations to derive the tracking force for this simplified problem. The analytic expression illustrates the effects of both electrostatic and magnetic tracking. As the conductivity approaches zero, Lee's expression is obtained.

The numerical simulations were carried out by the three-dimensional simulation code IPROP.² IPROP is a particle-in-cell code with air chemistry based on the Lawrence Livermore National Laboratory algorithm³ as modified by Science Applications International Corporation (SAIC).⁴ The code was used in the ultrarelativistic limit for a beam which is not allowed to respond dynamically (slug beam). In this case, the relatively small forces associated with tracking were easily identified. IPROP employs the full Maxwell equations without approximations such as those suggested by Lee⁵ and agrees well with the derived analytic result. The complete equations are necessary for the detailed study of channel tracking, since there is a

delicate balance between electrostatic and magnetic forces near the head of the beam.

As is shown later, the forces involved in channel tracking are only dominant fairly close to the head of the beam. Both magnetic and electrostatic components of the tracking force, observed in the numerical simulations, decay away several centimeters into the beam. The electrostatic force modeled by Lee¹ is created by the beam potential acting on the channel electrons. This produces a dipole force which tends to push the beam back toward the channel axis when the beam is displaced. The magnetic tracking force is due to the radial and azimuthal currents of the channel electrons which are driven by the beam potential as well as to the axial displacement current in Maxwell's equations. Since the distance from the beam head that a beam tracks has only a slight dependence on the rise time, short rise times and, hence, large displacement currents are desirable. For these beams tracking is dominated by the magnetic forces. Electrostatic forces dominate for longer rise times. It is for shorter rise times (<4 ns) that the full field equations are most needed.

Previous numerical work by Masamitsu⁶ and by Hui and Lampe⁷ using Lee's ultrarelativistic equations⁵ has given somewhat smaller values than IPROP for the tracking force in the short rise-time cases. IPROP has calculated forces an order of magnitude greater for a 0.5 ns rise-time beam than calculated by Hui and 2-3 times greater than Masamitsu. For a rise time of 4 ns, IPROP agrees reasonably well with Hui's results.⁸ Another interesting difference seen in the numerical simulations for a conductivity channel is the optimal initial conductivity for tracking. IPROP studies have indicated values as high as 3 (where conductivity is normalized as $4\pi a_b \sigma' / c$, where a_b is the beam Bennett radius and σ' is the scalar conductivity). Previous results have suggested a conductivity of 0.1. The higher values for conductivity and tracking may be accounted for by the different modeling of the magnetic fields in IPROP.

In Chapter 2, we will present analytic work which includes the tracking force derivation for the complete frozen-field equations. The numerical computations involving IPROP simulations are presented in Chapter 3. In Chapter 4, we discuss the physical interpretations of the results and give our conclusions in Chapter 5.

CHAPTER 2 ANALYTICAL MODELS

The electrostatic and magnetic dipole forces, acting on a displaced electron beam in a conductivity channel, nearly cancel close to the head of the beam. This is the crucial region which will determine whether or not the entire beam will track the channel, since the strong pinch force generally will cause the rest of the beam to follow the head. The complete field equations are necessary to fully understand what is happening in this region. In this section, we will consider a sharp-edged beam which is propagating entirely inside a square conductivity channel. A brief derivation of the resulting tracking force on the beam is given. The result is then used to check the accuracy of the code IPROP and compared with Lee's expression. All quantities will be given in cgs units with the tracking force given occasionally in gauss.

A. FROZEN-FIELD EQUATIONS

Maxwell's equations in an axially moving frame, when separated into forward- and backward-propagating components, are given by,⁹

$$\begin{aligned} \frac{1}{2} \left[\frac{\partial}{\partial t} + (c - v) \frac{\partial}{\partial z} \right] (E_r + B_\theta) + \frac{1}{2} \left[\frac{\partial}{\partial t} - (c + v) \frac{\partial}{\partial z} \right] (E_r - B_\theta) \\ + \sigma E_r = \frac{1}{r} \frac{\partial}{\partial \theta} B_z - J_z, \end{aligned} \quad (1)$$

$$\begin{aligned} \frac{1}{2} \left[\frac{\partial}{\partial t} + (c - v) \frac{\partial}{\partial z} \right] (E_r + B_\theta) - \frac{1}{2} \left[\frac{\partial}{\partial t} - (c + v) \frac{\partial}{\partial z} \right] (E_r - B_\theta) \\ = \frac{\partial}{\partial r} E_z, \end{aligned} \quad (2)$$

$$\begin{aligned} \frac{1}{2} \left[\frac{\partial}{\partial t} + (c - v) \frac{\partial}{\partial z} \right] (E_\theta - B_r) + \frac{1}{2} \left[\frac{\partial}{\partial t} - (c + v) \frac{\partial}{\partial z} \right] (E_\theta + B_r) \\ + \sigma E_\theta = - \frac{\partial}{\partial r} B_z - J_\theta, \end{aligned} \quad (3)$$

$$\begin{aligned} & \frac{1}{2} \left[\frac{\partial}{\partial t} + (c - v) \frac{\partial}{\partial z} \right] (E_\theta - B_r) - \frac{1}{2} \left[\frac{\partial}{\partial t} - (c + v) \frac{\partial}{\partial z} \right] (E_\theta + B_r) \\ &= \frac{1}{r} \frac{\partial}{\partial \theta} E_z, \end{aligned} \quad (4)$$

$$\begin{aligned} & \frac{1}{2} \left[\frac{\partial}{\partial t} + (c - v) \frac{\partial}{\partial z} \right] E_z + \frac{1}{2} \left[\frac{\partial}{\partial t} - (c + v) \frac{\partial}{\partial z} \right] E_z + \sigma E_z \\ &= \frac{1}{r} \frac{\partial}{\partial r} r B_\theta - \frac{1}{r} \frac{\partial}{\partial \theta} B_r - J_z, \end{aligned} \quad (5)$$

and,

$$\begin{aligned} & \frac{1}{2} \left[\frac{\partial}{\partial t} + (c - v) \frac{\partial}{\partial z} \right] B_z + \frac{1}{2} \left[\frac{\partial}{\partial t} - (c + v) \frac{\partial}{\partial z} \right] B_z \\ &= -\frac{1}{r} \frac{\partial}{\partial r} r E_\theta + \frac{1}{r} \frac{\partial}{\partial \theta} E_r, \end{aligned} \quad (6)$$

where c and v are the speed of light and the reference frame velocity, respectively, and $\sigma = 4\pi\sigma'/c$.

The frozen-field equations are obtained by setting $v = c$ and dropping time derivatives. With some manipulation, the frozen-field equations become

$$E_r = \frac{1}{\sigma} \left(\frac{\partial}{\partial r} E_z + \frac{1}{r} \frac{\partial}{\partial \theta} B_z \right), \quad (7)$$

$$E_\theta = -\frac{1}{\sigma} \left(\frac{\partial}{\partial r} B_z - \frac{1}{r} \frac{\partial}{\partial \theta} E_z \right), \quad (8)$$

$$\frac{\partial}{\partial \tau} B_r = \frac{\partial}{\partial \tau} \frac{1}{\sigma} \frac{\partial}{\partial r} B_z - \left(1 + \frac{\partial}{\partial \tau} \frac{1}{\sigma} \right) \frac{1}{r} \frac{\partial}{\partial \theta} E_z, \quad (9)$$

$$\frac{\partial}{\partial \tau} B_\theta = \left(1 + \frac{\partial}{\partial \tau} \frac{1}{\sigma} \right) \frac{\partial}{\partial r} E_z + \frac{\partial}{\partial \tau} \frac{1}{\sigma} \frac{1}{r} \frac{\partial}{\partial \theta} B_z, \quad (10)$$

$$\begin{aligned} & \frac{\partial}{\partial \tau} \left(\frac{\partial}{\partial \tau} + \sigma \right) E_z = \left[\frac{1}{r} \frac{\partial}{\partial r} r \left(1 + \frac{\partial}{\partial \tau} \frac{1}{\sigma} \right) \frac{\partial}{\partial r} + \frac{1}{r} \frac{\partial}{\partial \theta} \left(1 + \frac{\partial}{\partial \tau} \frac{1}{\sigma} \right) \right. \\ & \left. \frac{1}{r} \frac{\partial}{\partial \theta} \right] E_z + \frac{\partial}{\partial \tau} \left[\frac{1}{r} \frac{\partial}{\partial r} r \frac{1}{\sigma} \frac{1}{r} \frac{\partial}{\partial \theta} - \frac{1}{r} \frac{\partial}{\partial \theta} \frac{1}{\sigma} \frac{\partial}{\partial r} \right] B_z - \frac{\partial}{\partial \tau} J_z, \end{aligned} \quad (11)$$

and,

$$\begin{aligned} \frac{\partial}{\partial \tau} B_z = & \left[\frac{1}{r} \frac{\partial}{\partial r} r \frac{1}{\sigma} \frac{\partial}{\partial r} + \frac{1}{r} \frac{\partial}{\partial \theta} \frac{1}{\sigma} \frac{1}{r} \frac{\partial}{\partial r} \right] B_z \\ & - \left[\frac{1}{r} \frac{\partial}{\partial r} r \frac{1}{\sigma} \frac{1}{r} \frac{\partial}{\partial \theta} - \frac{1}{r} \frac{\partial}{\partial \theta} \frac{1}{\sigma} \frac{1}{r} \frac{\partial}{\partial r} \right] E_z \end{aligned} \quad (12)$$

with $\tau = -z/c$.

When σ is constant, Eqs. 11 and 12 simplify greatly into uncoupled second-order equations:

$$\left(\frac{\partial}{\partial \tau} + \sigma \right) \left(\sigma \frac{\partial}{\partial \tau} - \frac{1}{r} \frac{\partial}{\partial r} r \frac{\partial}{\partial r} - \frac{1}{r^2} \frac{\partial^2}{\partial \theta^2} \right) E_z = -\sigma \frac{\partial}{\partial \tau} J_z \quad (13)$$

and

$$\left(\sigma \frac{\partial}{\partial \tau} - \frac{1}{r} \frac{\partial}{\partial r} r \frac{\partial}{\partial r} - \frac{1}{r^2} \frac{\partial^2}{\partial \theta^2} \right) B_z = 0. \quad (14)$$

Furthermore, Eq. 13 can be integrated yielding,

$$\left(\sigma \frac{\partial}{\partial \tau} - \frac{1}{r} \frac{\partial}{\partial r} r \frac{\partial}{\partial r} - \frac{1}{r^2} \frac{\partial^2}{\partial \theta^2} \right) E_z = -\sigma e^{-\sigma \tau} \int e^{\sigma \tau'} \frac{\partial}{\partial \tau'} J_z d\tau'. \quad (15)$$

We now have six equations, Eqs. 7-10, 14 and 15, valid for a constant conductivity region in the frozen-field limit.

B. DERIVATION OF THE TRACKING FORCE

We will solve the above equations for a channel with a square conductivity profile (constant σ inside $r = a$ and zero elsewhere). The tracking force is obtained for an electron beam propagating totally inside the channel. The equations are Fourier analyzed (simply replace second-order differentials with respect to θ with $-m^2$) in order to determine the dipole force acting on the beam (force in the $m = 1$ mode). The only approximation will be to neglect the $\sigma d/d\tau$ term in Eqs. 14 and 15 for $r < a$. For $\sigma^2 a^2 \ln(b/a) < 4$, where b is the drift tube radius, this term was found to

be important only at the boundary of the channel and must be kept in the boundary conditions. The sudden build-up of surface charges and currents at $r = a$ is responsible for the significance of the term, particularly near the beam head. To reduce the error in calculating the dipole force, we will analytically subtract out the forces symmetric about the beam by separating the fields into beam- and channel-symmetric components.

We can quickly solve the $m = 1$ mode equations outside the channel with no approximation, since the $\sigma d/d\tau$ term is identically 0. The $m = 1$ fields, where the superscript (1) denotes $m = 1$ quantities, are

$$E_z^{(1)} = B_z^{(1)} = a \frac{\partial}{\partial \tau} \gamma (r/a)^{-1} \quad (16a)$$

$$E_\theta^{(1)} = a^2 \frac{\partial^2}{\partial \tau^2} \gamma \ln b/r + \frac{1}{2} (\gamma + \delta) (r/a)^{-2} \quad (16b)$$

and,

$$B_\theta^{(1)} = -a^2 \frac{\partial^2}{\partial \tau^2} \gamma \ln b/r - \frac{1}{2} (\gamma - \delta) (r/a)^{-2} \quad (16c)$$

for $b > a$, where γ and δ are τ -dependent only.

The boundary conditions are determined from the complete frozen-field equations (Eqs. 7-12) by evaluating them at $r = a$. The useful boundary conditions to the derivation are

$$E_z \text{ continuous at } a \quad (17a)$$

$$B_z \text{ continuous at } a \quad (17b)$$

$$E_z^{(1)}(a) = B_z^{(1)}(a) \quad (17c)$$

and,

$$\frac{\partial}{\partial \tau} (E_\theta^{(1)} - B_\theta^{(1)}) = -\frac{1}{\sigma} \frac{\partial}{\partial \tau} \left(\frac{\partial}{\partial r} + \frac{1}{r} \right) (E_z^{(1)} + B_z^{(1)}) - \frac{\partial}{\partial r} E_z^{(1)}, \quad (17d)$$

which results from the continuity of $E_\theta^{(1)} - B_\theta^{(1)}$. The advantages of the last boundary condition will be more obvious later.

Taking $\sigma d/d\tau = 0$ inside the channel, we can immediately determine B_z from Eq. 14,

$$B_z^{(1)} = a \frac{\partial}{\partial \tau} \gamma(r/a) \quad (18)$$

where the continuity of B_z has been used. Splitting the fields into beam- and channel-symmetric parts, we express E_z as

$$E_z^{(1)} = a \frac{\partial}{\partial \tau} A^{(1)}(r) + a \frac{\partial}{\partial \tau} \alpha(r/a), \quad (19)$$

where α is dependent only on τ . This is helpful, since only the second term in Eq. 19 need be considered when calculating the tracking force.

To obtain $A^{(1)}$, we first consider the case where both the beam and channel are symmetric about the z axis ($m = 0$). From Eq. 15, the solution is

$$\frac{\partial}{\partial \tau} A^{(0)} = \sigma e^{-\sigma \tau} \int_0^\tau d\tau' e^{\sigma \tau'} \frac{\partial}{\partial \tau'} I_z \ln(r^2/a^2), \quad (20)$$

where I_z is the total current. The $m = 1$ solution is obtained by displacing the beam by ϵ . When ϵ is small, we get

$$\frac{\partial}{\partial \tau} A^{(1)}(a) = \frac{-2\epsilon}{a} \sigma e^{-\sigma \tau} \int_0^\tau d\tau' e^{\sigma \tau'} \frac{\partial}{\partial \tau'} I_z. \quad (21)$$

We can now solve for α by noting δ drops out of the fourth boundary condition (Eq. 17d) and then solving for α in terms of the known $A^{(1)}(a)$. After a great deal of algebra, we obtain

$$\alpha = \frac{-X}{\sqrt{1-X}} e^{-\sigma\tau/X} \int_0^\tau d\tau' \left(\sinh \frac{\sqrt{1-X}}{X} \sigma(\tau - \tau') \right) \frac{\partial}{\partial \tau'} e^{\sigma\tau'/X} \frac{\partial}{\partial \tau'} A^{(1)}(a) \quad (22a)$$

where

$$X = \sigma^2 a^2 \ln(b/a) . \quad (22b)$$

The tracking force for a small beam displacement is given by

$$F_t = \frac{1}{2} \int (E_r - B_\theta - E_\theta - B_r)^{(1)} J_z r dr , \quad (23)$$

where only terms involving α need to be considered. Again, after much algebra, we obtain the tracking force per current:

$$\frac{F_t}{I_z} = \frac{2\epsilon}{a^2} \int_0^\tau d\tau' i_z \left[-e^{-\sigma(\tau-\tau')} + e^{-\sigma(\tau-\tau')/X} \left(\cosh \frac{\sqrt{1-X}}{X} \sigma(\tau - \tau') + \frac{1}{\sqrt{1-X}} \sinh \frac{\sqrt{1-X}}{X} \sigma(\tau - \tau') \right) \right] . \quad (24)$$

where we adopt the convention that a positive force indicates tracking. The tracking force is proportional to ϵ/a^2 and is independent of the other spatial characteristics of the beam. Eq. 24 is valid up to about $X = 4$, where the $\sigma d/d\tau = 0$ approximation breaks down.

C. RESULTS

The physics of channel tracking is best understood by separating the tracking force into electrostatic and magnetic components. These are obtained from Eq. 22 and are given by

$$\frac{F_e}{I_z} = \frac{2\epsilon}{a^2} \int_0^\tau d\tau' \dot{I}_z \left[-e^{-\sigma(\tau-\tau')} + e^{-\sigma(\tau-\tau')/\chi} \frac{2}{\sqrt{1-\chi}} \sinh \frac{\sqrt{1-\chi}}{\chi} \sigma(\tau - \tau') \right] \quad (25)$$

and,

$$\frac{F_b}{I_z} = \frac{2\epsilon}{a^2} \int_0^\tau d\tau' \dot{I}_z e^{-\sigma(\tau-\tau')/\chi} \left[\cosh \frac{\sqrt{1-\chi}}{\chi} \sigma(\tau - \tau') - \frac{\sqrt{1-\chi}}{\chi} \sinh \frac{\sqrt{1-\chi}}{\chi} \sigma(\tau - \tau') \right] \quad (26)$$

The electrostatic force behavior is described by the build up of charge at the channel boundary and its subsequent decay. In Eq. 25, the first term in the integral controls the build up of charge at the channel boundary. This term decays as $\exp(-\sigma\tau)$. The second term controls the charge decay from $r = a$, and, for $\chi = 0$, decays more slowly as $\exp(-\sigma\tau/2)$. Thus, in the limit of $\chi = 0$, the charge builds up indefinitely for positive $dI_z/d\tau$.

The first and second terms in the magnetic force equation correspond closely to those of Eq. 25. The first term describes the effects of the transverse outward currents, which are responsible for the growth of the channel surface charge, and the dipole axial displacement current ($dE_z^{(1)}/d\tau$) caused by the resulting asymmetric channel electrons. Both effects are responsible for the transverse magnetic fields which cause tracking. The second term controls the transverse return currents which drain the surface charge and cause detracking. Electrostatic and magnetic forces are, therefore, intimately related. Note that, for $\chi > 1$, the solutions to Eqs. 25 and 26 become oscillatory. In this case, the transverse currents alternate direction as they decay.

Now, we will consider a 10-kA beam offset 1/4 cm in a 1-cm channel with constant $\sigma = 0.2 \text{ cm}^{-1}$. The time-dependent beam current is given by

$$I_z = I_0 (1 - \exp(-\beta\tau)) \quad (27)$$

where $1/\beta$ is the current rise time which we will take as 15 cm here. The resulting tracking forces, F_e , F_b and the total force, are plotted in Figure 1 for $b = 25$ cm. We see at the beam head ($\tau = 0$), the magnetic force is dominant with the electric force giving detracking (negative force). Later on, as the channel electrons are able to redistribute themselves (this takes place on time scale $1/\sigma$), the electrostatic force begins to dominate. As expected, this occurs at $\tau = 5$ cm in Figure 1. The magnetic force decays and eventually becomes detracking at $\tau = 12$ cm. If the conductivity is sufficient, the magnetic detracking will eventually dominate.

We found that IPROP (using the same channel geometry and beam as the analytic model) is in good agreement (within 10%) with the derived expression for the total tracking force for $X < 4$. In Figures 2a and 2b, the tracking force, on the same beam as above, is calculated using IPROP and the analytic model. In this case, the 1-cm radius channel has a 0.5-cm^{-1} conductivity ($X = 1$). In Figure 2a, the total tracking forces calculated using IPROP and the model are very close particularly near the beam head. When the force is separated into its electric and magnetic components (Figure 2b), the agreement is good until the magnetic component becomes relatively small. This deviation results from the neglect of the $\sigma d/d\tau$ terms in Eqs. 14 and 15. This term may be important to an individual component of the force if its magnitude is small compared to the total force. For $X > 4$, neglecting the $\sigma d/d\tau$ term is no longer valid, and the total force calculated analytically deviates from IPROP. The good agreement of IPROP to the rigorously derived analytic expression for smaller X gives us confidence in the accuracy of IPROP, which will be used extensively in the next section.

We will now compare our new expression with Lee's for the above example with varying X (actually, the conductivity and the channel radius will remain constant while we vary the drift tube radius). The total tracking force obtained from Eq. 24 for current profile 27 is

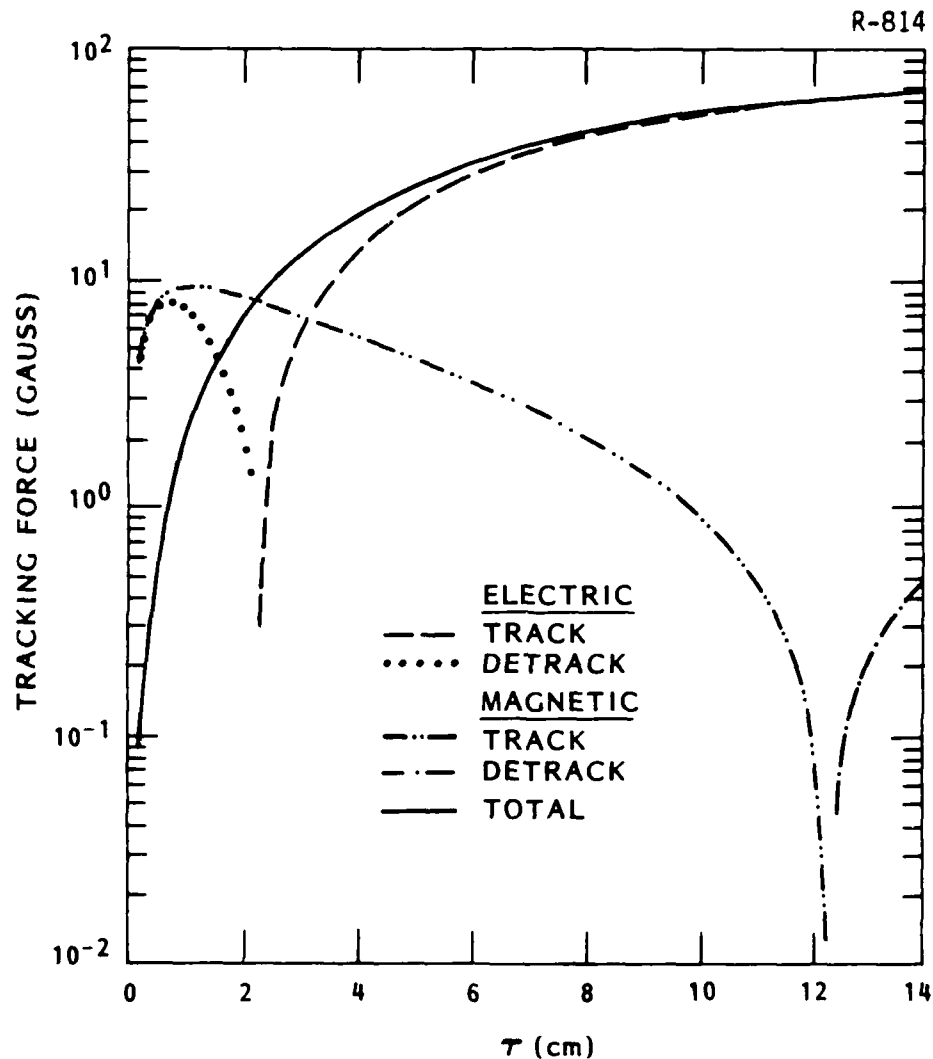


Figure 1. The total tracking force with the electric and magnetic components, calculated for an electron beam using the analytic model, are plotted versus the beam coordinate, r . The 10-kA beam with a 0.25-cm displacement propagates through a 1-cm radius channel with 0.2-cm⁻¹ conductivity.

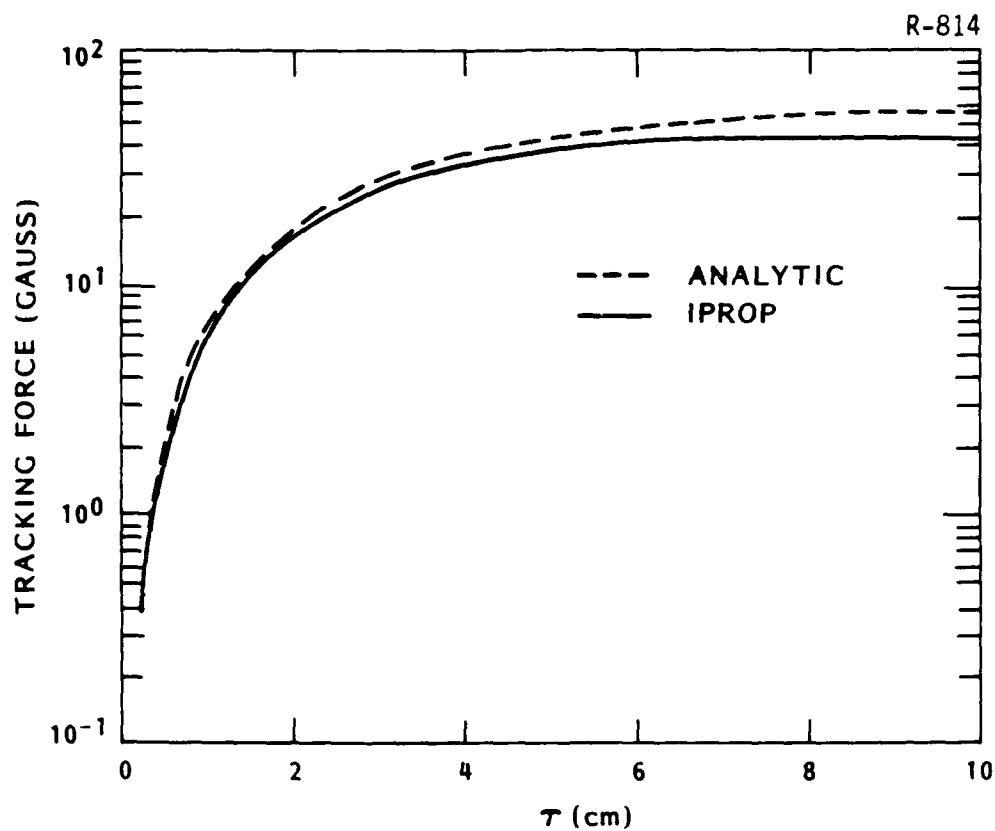
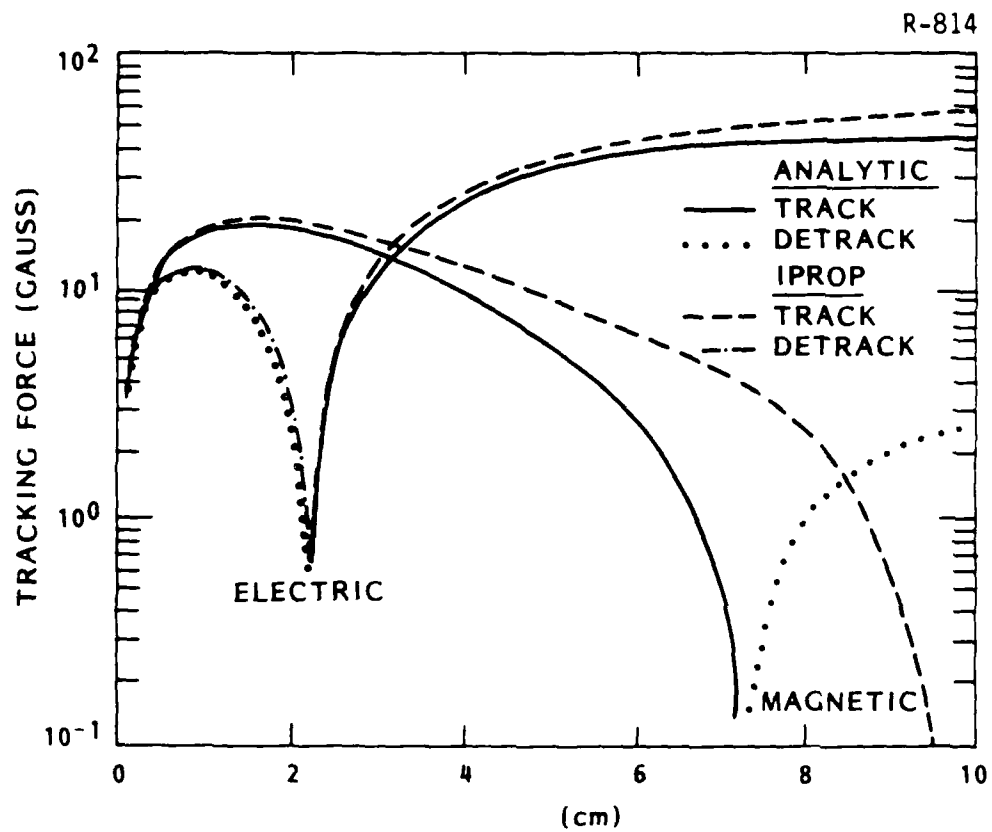


Figure 2. The tracking force, on a 10-kA beam with a 15-cm rise time in a 1-cm channel with $\sigma = 0.5 \text{ cm}^{-1}$, is plotted using the results from the analytic model and IPROP. In (a), the total force is given and, in (b), the electric and magnetic components of the force are plotted. Note the good agreement when the forces are relatively large.



(b)

Figure 2. Concluded.

$$\begin{aligned}
\frac{F_t}{I_z} = \frac{2\epsilon I_0}{a^2} \beta & \left[\frac{1}{\beta - \sigma} (e^{-\beta\tau} - e^{-\sigma\tau}) + \frac{1}{2} \frac{1 + (1 - X)^{-1/2}}{\sigma/X(1 - \sqrt{1 - X}) - \beta} \right. \\
& \times \left(e^{-\beta\tau} - e^{(\sqrt{1-X}-1)\sigma\tau/X} \right) + \frac{1}{2} \frac{1 - (1 - X)^{1/2}}{\sigma/X(1 + \sqrt{1 - X}) - \beta} \\
& \left. \left(e^{-\beta\tau} - e^{-(\sqrt{1-X}+1)\sigma\tau/X} \right) \right]. \quad (28)
\end{aligned}$$

For the same case, Lee's expression is given by,

$$\frac{F_t}{I_z}^{\text{Lee}} = \frac{2\epsilon I_0}{a^2} \left[\frac{\beta e^{-\sigma\tau/2} - (\sigma/2)e^{-\alpha\tau}}{\beta - \sigma/2} - \frac{\beta e^{-\sigma\tau} - \sigma e^{-\beta\tau}}{\beta - \sigma} \right] \quad (29)$$

It should be noted that Eq. 28 limits to Lee's expression in the limit of small X . This is illustrated in Figure 3 where Eq. 28 is plotted for $X = 1, 2$ and 5 , while holding $\sigma = 1 \text{ cm}^{-1}$ and $a = 1 \text{ cm}$. Since Lee's model neglects magnetic effects which become important for increasing X , Eq. 28 deviates from Lee's expression at large X . At early times (small τ), the magnetic tracking of the full-equation expression, seen in Figure 1, results in larger tracking. Later, as the dipole charge builds and the electrostatic component becomes dominant, the total force approaches that of the purely electrostatic expression of Lee. Note the distinct oscillation in the tracking force (for $X = 5$) which was predicted earlier for $X > 1$. In this example, we varied the drift tube radius to change X . However, the same deviation is seen when σ is increased and a and b are held constant.

Finally, we consider the rise-time dependence of Eq. 28. In Figure 4, we see the peak tracking force plotted versus rise time. As the rise time decreases to 30 cm , the tracking force rises sharply. However, as the rise time approaches the inverse of the channel conductivity (5 cm), the increase in tracking is slowed. This is caused by the channel electrons being unable to respond to the sharp current rise. This creates an optimal force of 76 gauss as the rise time approaches zero.

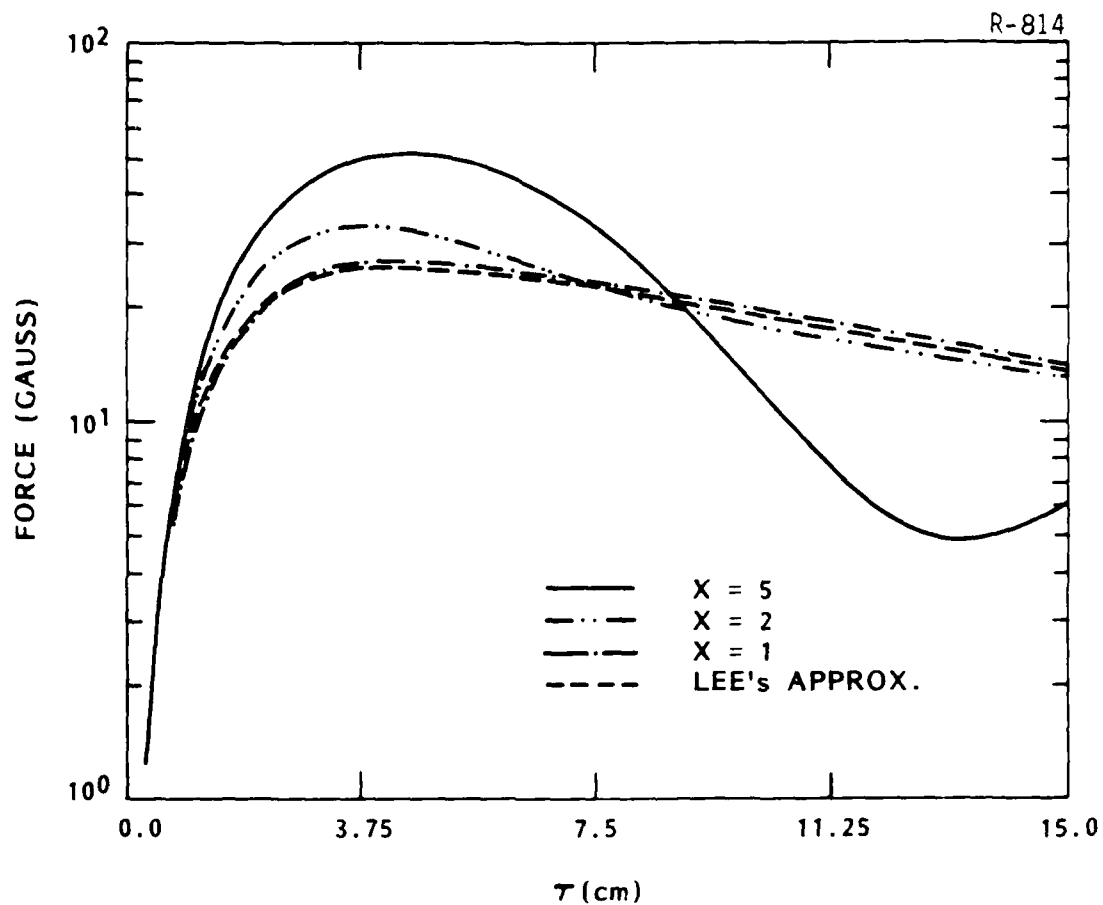


Figure 3. The tracking force on a 10-kA beam with a 0.25-cm displacement is calculated using the analytic model with $X = 1, 2$ and 5 and compared with Lee's expression. The 1-cm channel has $\gamma = 1 \text{ cm}^{-1}$. The drift-tube radii are 2.7, 7.4 and 150, corresponding to $X = 1, 2$ and 5 , respectively.

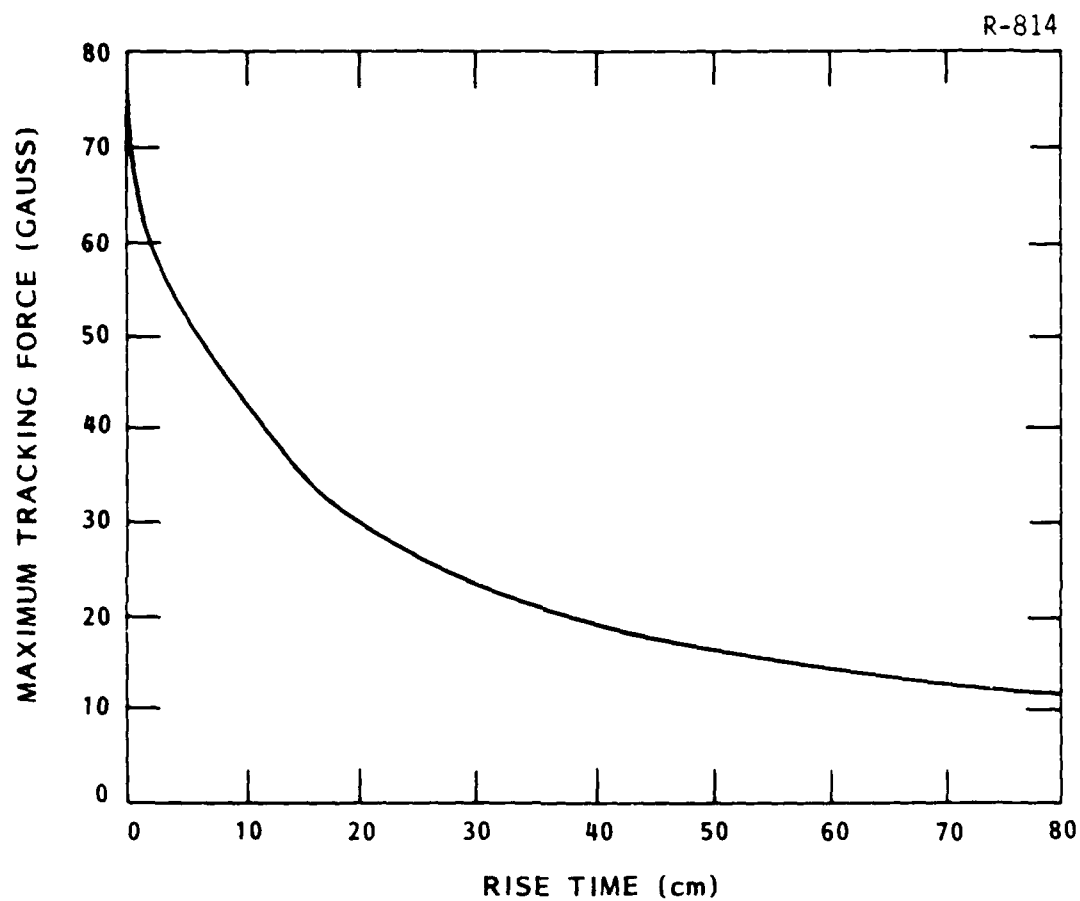


Figure 4. The maximum tracking force on a 10-kA beam in a 1-cm channel with $\mu = 0.2 \text{ cm}^{-1}$ is plotted for variable beam rise time.

The derived analytic expression illustrates the balance between electrostatic and magnetic forces as well as giving us a check on IPROP's behavior. The key addition to the complete frozen-field equations is the axial displacement current which drives large dipole magnetic fields near the beam head. These fields guide the beam back towards the z axis. IPROP agrees well with the analytic model using the same beam/channel geometry. We anticipate, therefore, that in a realistic beam/channel configuration where magnetic tracking dominates, IPROP should yield reliable results which may differ markedly from those of Lee's ultrarelativistic equations.

CHAPTER 3 NUMERICAL SIMULATIONS

The results from the code IPROP studies, involving a more complex channel and electron beam, are presented in this section. The three types of channels considered are conductivity, density and conductivity/density (combination). The radial profiles of the channels are Gaussian with conductivity and/or density given in terms of the channel-symmetric coordinate r' as

$$\sigma = \sigma_0 \exp(-(r'/r_c)^2) \quad (30a)$$

and

$$n = n_{\text{amb}} - n_d \exp(-(r'/r_c)^2) \quad , \quad (30b)$$

where σ_0 , n_{amb} and n_d are the maximum channel conductivity, ambient pressure in atmospheres and the depth of the density channel, respectively.

The beam has a 50-MeV energy (the energy is used only in the air chemistry routine in IPROP) and a Bennett profile with current density given by

$$J_z(r) = \frac{J_0 a_b^4}{(a_b^2 + r^2)^2} \quad , \quad (31)$$

where J_0 is the on-axis current density. We will consider both pencil- and trumpet-shaped beams. The r -dependent current profile is again given by Eq. 27. The beam will not be allowed to respond dynamically to the channel forces.

The simulation code IPROP is finite differenced in the z and r directions and Fourier-analyzed in M number of modes in the θ direction. We

have run the code with both channel and beam off the z axis. The two cases agree to within 10% for small displacements ($<0.5 a_b$). We found it advantageous to run the code with the channel offset, since a smaller number of θ modes and, hence, less computer time and memory are needed. The number of modes is dependent on the displacement divided by the width of the object displaced (the channel or the beam), and the channel is generally wider than the beam. For moderate channel offsets ($<1.5 r_c$), 2-4 modes are sufficient to determine the tracking force accurately in the channel-offset case. In this case, the tracking force was also less sensitive to b (drift tube radius set at 25 cm here) than in the offset beam case.

The conductivity in IPROP evolves due to impact ionization, electron avalanche (generated by the electric fields) and recombination based on the SAIC algorithm. An energy-dependent momentum-transfer cross section also is used. A critical numerical parameter in the code is the cell size in the z direction. We found that, for the initial conductivities used ($\leq 5 \text{ cm}^{-1}$), the results were insensitive to change in the cell size for values less than 0.25 cm.

A. PENCIL BEAM

We first consider a typical pencil-beam case for the three channel types. The beam, again, has a 10-kA peak current with a 15-cm rise time and $a_b = 0.5 \text{ cm}$. The 1-cm channels are offset $3/4 \text{ cm}$ and have 0.2 cm^{-1} conductivity and $n_d = 0.9 \text{ atm}$ (a minimum density of 0.1 atm for $n_{\text{amb}} = 1 \text{ atm}$). In Figure 5, the tracking force on a beam slice (defined in Eq. 23) per current is plotted for the three cases. For all cases, the beam tracks for approximately 5 cm, with the conductivity channel tracking longest. The highest tracking is found in the conductivity/density channel at 15 gauss.

The density channel differs from the conductivity channel in that the tracking is almost totally magnetic with the significant electric forces

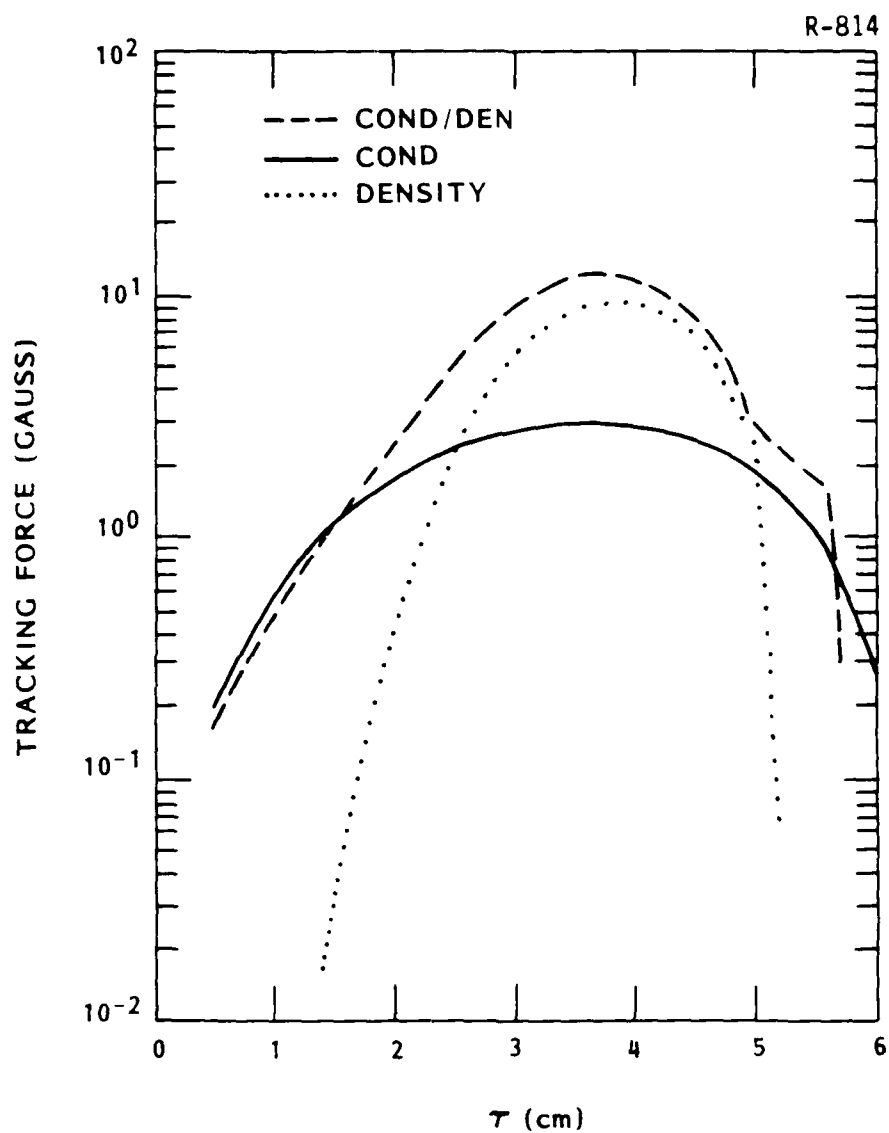


Figure 5. The tracking force, calculated using IPROP, is sketched versus r . The channels considered are conductivity, density and combination (conductivity/density). The 10-kA, 50-MeV beam has a 0.5-cm radius with a Bennett profile. The Gaussian-shaped channel has $r_c = 1$ cm.

being detracking through 6 cm. Figures 6 and 7 break the tracking force of the conductivity and density channels, respectively, into its electrostatic and magnetic components. Note the tracking force is completely magnetic in the conductivity channel up to 4 cm into the beam, although the increasing electric component is responsible for the longer tracking. In the density channel, the electric force is detracking except at the very head where it reaches only 0.4 gauss. This magnetic dominance is typical for short rise-time beams.

The channel electrons have time to respond and cause electrostatic tracking when the rise time increases. Figure 8 sketches the tracking behavior of a 120-cm rise-time beam for a conductivity channel. The contribution of the electric forces are now becoming comparable to the magnetic forces. Both the electric and magnetic components cause detracking at 12 cm with the return-current magnetic detracking dominating. In the density channel case, the magnetic forces will generally dominate since the conductivity is too localized near regions of high electric field to significantly rearrange the channel electrons and cause electrostatic tracking.

By varying the initial conductivity, we found the optimal tracking force for a variety of beam/channel parameters. In Table 1, the conductivity which produced the maximum tracking force for a conductivity channel is given. The nominal parameters are:

$$\epsilon = 0.75 \text{ cm},$$

$$r_c = 1 \text{ cm},$$

$$a_b = 0.5 \text{ cm},$$

$$I_0 = 10 \text{ kA},$$

and,

$$1/\beta = 15 \text{ cm}.$$

In Table 1, the beam and channel are always nominal unless specified otherwise.

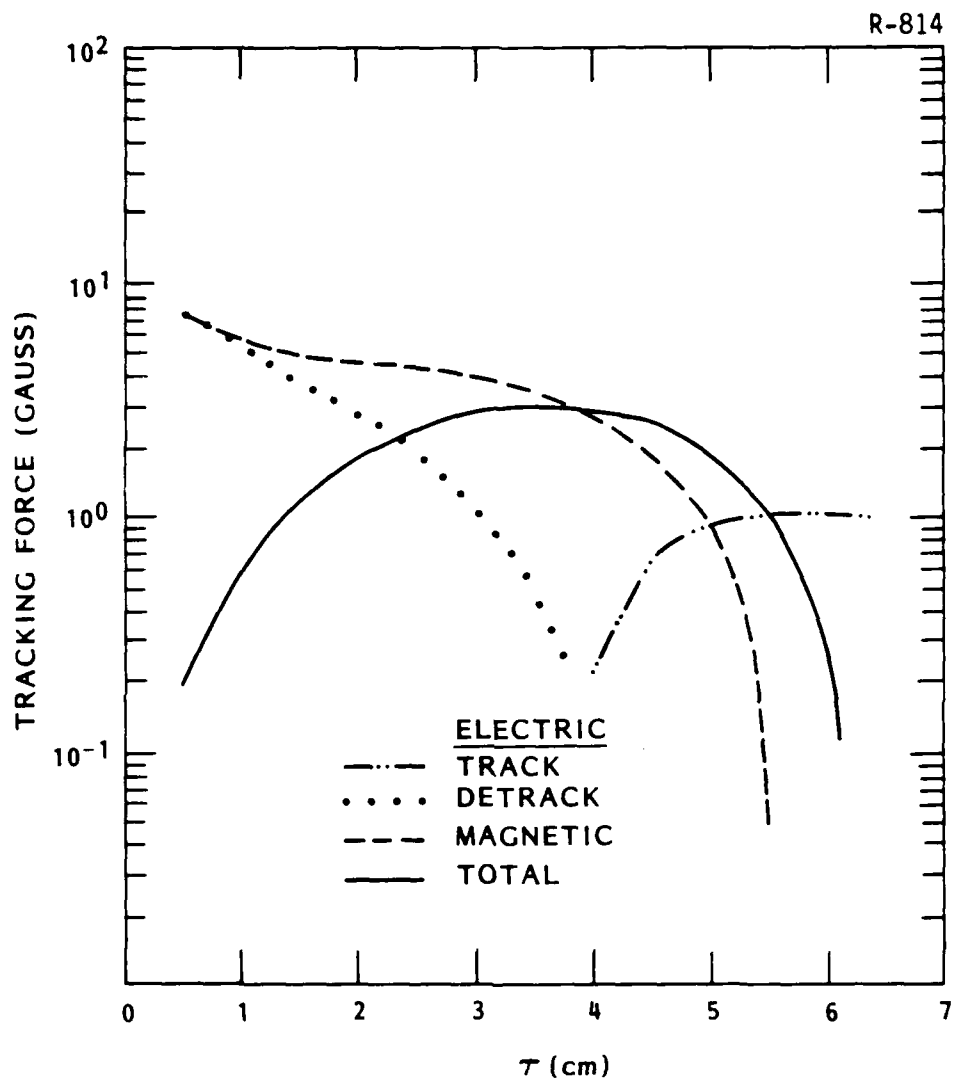


Figure 6. The electric and magnetic components of the total tracking force are plotted for a 10-kA beam with a 15-ns rise time in a 1-cm conductivity channel.

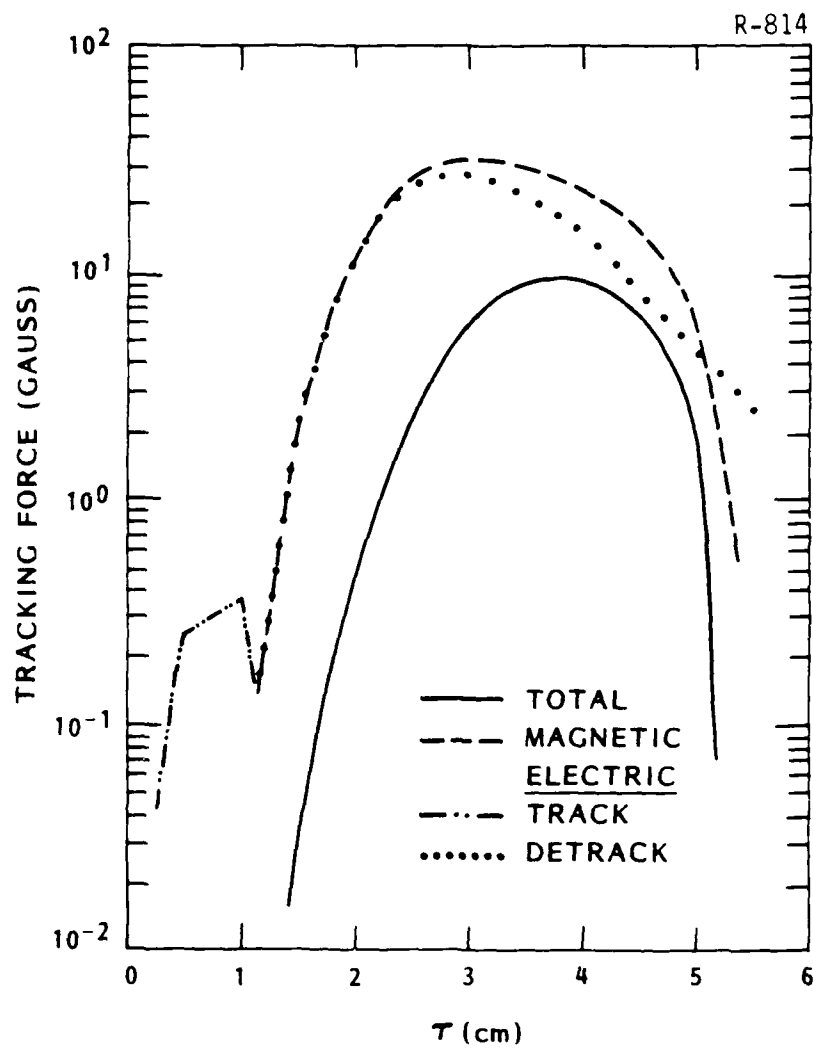


Figure 7. The electric and magnetic components of the total tracking force are plotted for a 10-kA beam with a 15-ns rise time in a 1-cm density channel.

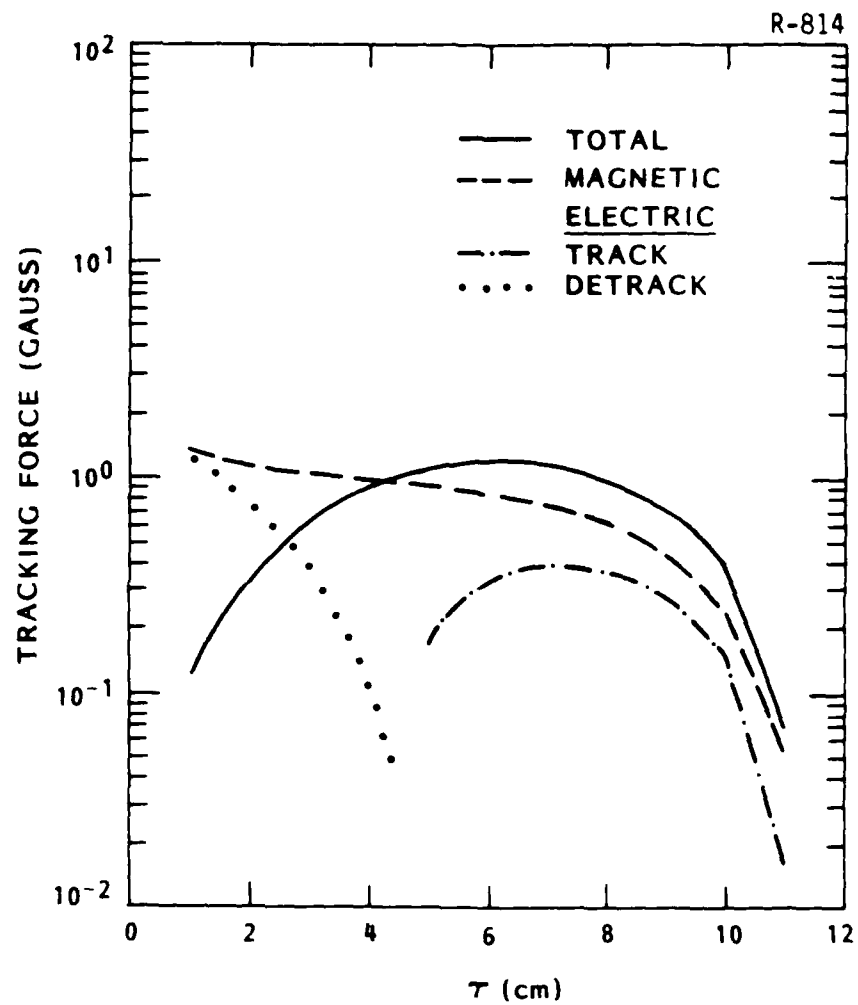


Figure 8. The electric and magnetic components of the total tracking force are plotted for a 10-kA beam with a 120-ns rise time in a 1-cm density channel.

TABLE 1. OPTIMIZATION OF CHANNEL TRACKING IN CONDUCTIVITY CHANNEL.

<u>Varied Parameter and Its Value</u>	<u>Optimal σ_0 (cm^{-1})</u>	<u>Maximum Tracking Force (gauss)</u>
Nominal	4.7	24.8
$a_b = 0.25 \text{ cm}$	4.4	46.3
$a_b = 1.0 \text{ cm}$	5.0	4.5
$I_0 = 1 \text{ kA}$	3.0	3.2
$I_0 = 5 \text{ kA}$	3.5	13.2
$r_c = 2.0 \text{ cm}$	1.6	17.5
$r_c = 3.0 \text{ cm}$	1.0	11.3
$1/\beta = 30 \text{ cm}$	4.0	15.3
$1/\beta = 60 \text{ cm}$	3.5	9.0
$\epsilon = 0.25 \text{ cm}$	3.6	8.7
$\epsilon = 0.50 \text{ cm}$	4.2	17.0
$\epsilon = 1.50 \text{ cm}$	5.0	36.6

The values for optimal σ_0 and F_t are surprisingly high. For nominal parameters, a tracking force of 25 gauss for 4.7-cm^{-1} conductivity was calculated. As predicted in the analytic model derived in the second section, F_t increases approximately as $\epsilon I_0 B / r_c^2$. The optimal σ_0 changes particularly when r_c is varied. This phenomenon is not fully modeled by the analytic expression, since the beam was restricted to be entirely within the channel and conductivity generation was not considered. We see the optimal σ_0 decreases by a factor of 5 as r_c increases from 1 to 3 cm. Another result not predicted by the model is the a_b dependence. The tracking force increases an order of magnitude as a_b decreases from 1 to 1/4 cm, probably because a greater portion of the Bennett-profile beam lies within the channel for a smaller Bennett radius. With the maximum tracking force over 40 gauss, these results are much more optimistic than those previously documented.

In Table 2, the IPROP results are summarized for the density channel case. Here, the optimized parameter is the displacement. As seen by Hui and Lampe⁷, the beam will not track until the channel is approximately $1/2 r_c$ off axis. The optimal ϵ for nominal parameters is 1.5 cm. This value varies little unless r_c or a_b are changed. We find the optimal displacement scales as,

$$\epsilon_{\text{opt}} \sim r_c + a_b . \quad (32)$$

This scaling is caused by the peak electric field occurring near the edge of the beam. Since the avalanche-produced conductivity grows as a function of E^2/n^2 , the tracking occurs only when the beam is well off axis allowing one beam edge to lie near the channel center. There is a similar scaling of F_t with a_b , I_0 and rise time as in the conductivity case with tracking about half as great. For optimal displacement, IPROP calculates a 15 gauss tracking force.

Finally, we examine the density/conductivity channel in Table 3. The results are similar to those of the conductivity channel with one

TABLE 2. OPTIMIZATION OF TRACKING IN DENSITY CHANNEL.

<u>Varied Parameter and Its Value</u>	<u>Optimal ϵ (cm)</u>	<u>Maximum Tracking Force (gauss)</u>
Nominal	1.5	14.8
$a_b = 0.25$ cm	1.2	21.0
$a_b = 1.0$ cm	2.0	4.3
$I_0 = 1$ kA	1.5	0.39
$I_0 = 5$ kA	1.5	7.8
$r_c = 2$ cm	2.5	14.8
$r_c = 3$ cm	4.6	5.9
$1/\beta = 30$ cm	1.5	9.1
$1/\beta = 60$ cm	1.5	3.5

TABLE 3. OPTIMIZATION OF TRACKING IN DENSITY/CONDUCTIVITY CHANNEL.

<u>Varied Parameter and Its Value</u>	<u>Optimal σ_0 (cm⁻¹)</u>	<u>Maximum Tracking Force (gauss)</u>
Nominal	4.5	20.6
$a_b = 0.25$ cm	3.2	33.6
$a_b = 1.0$ cm	5.1	5.6
$I_0 = 1$ kA	2.9	3.1
$I_0 = 5$ kA	4.3	13.5
$r_c = 1.5$ cm	1.6	13.0
$r_c = 2.0$ cm	0.84	8.2
$1/\beta = 30$ cm	4.3	14.2
$1/\beta = 60$ cm	3.4	8.5
$\epsilon = 1.5$ cm	4.6	34.4
$\epsilon = 2.0$ cm	4.8	37.1

qualification. At $\epsilon = 0.75$ cm, the detracking effects of the density channel near the axis produce smaller F_t . We see that when the displacement is increased to 1.5 cm, the tracking force nearly catches up to the conductivity case. Clearly, at these high conductivities the detracking effects of the depressed density in the combination channel make it less desirable than the pure conductivity channel.

B. TRUMPET BEAM

The trumpet-shaped beam is a more realistic representation of a laboratory beam and must be given some attention here. We will not go into as much detail as in the pencil case, since the results are qualitatively similar. As one would expect from the beam radius dependence of a pencil beam, the tracking for a trumpet beam is much smaller. The trumpet shape used in IPR0P scales the Bennett radius to τ as,

$$a_b(\tau) = 0.5 \text{ cm} + c_1 \exp(-\tau/c_2) \quad (33)$$

where $c_1 = 6$ cm and $c_2 = 8$ cm. The current variation is still described by Eq. 27.

In Figure 9, the tracking force of a trumpet beam in a 3-cm channel is compared with that of a pencil beam with $a_b = 2$ cm for a channel with a 0.2-cm^{-1} conductivity. The 2-cm radius is the average trumpet beam radius during its tracking period. The maximum tracking for the trumpet beam occurs roughly at the same position in the beam as the pencil beam with half the force. The initial force for the pencil is much greater, since the trumpet is over 3 times wider. The magnetic detracking of the trumpet beam is much stronger further back in the beam, causing a quicker decline than the pencil beam at $\tau = 13$ cm. Despite these differences, the tracking behavior with respect to channel offset, radius, peak beam current and rise time is similar to the wide pencil beam.

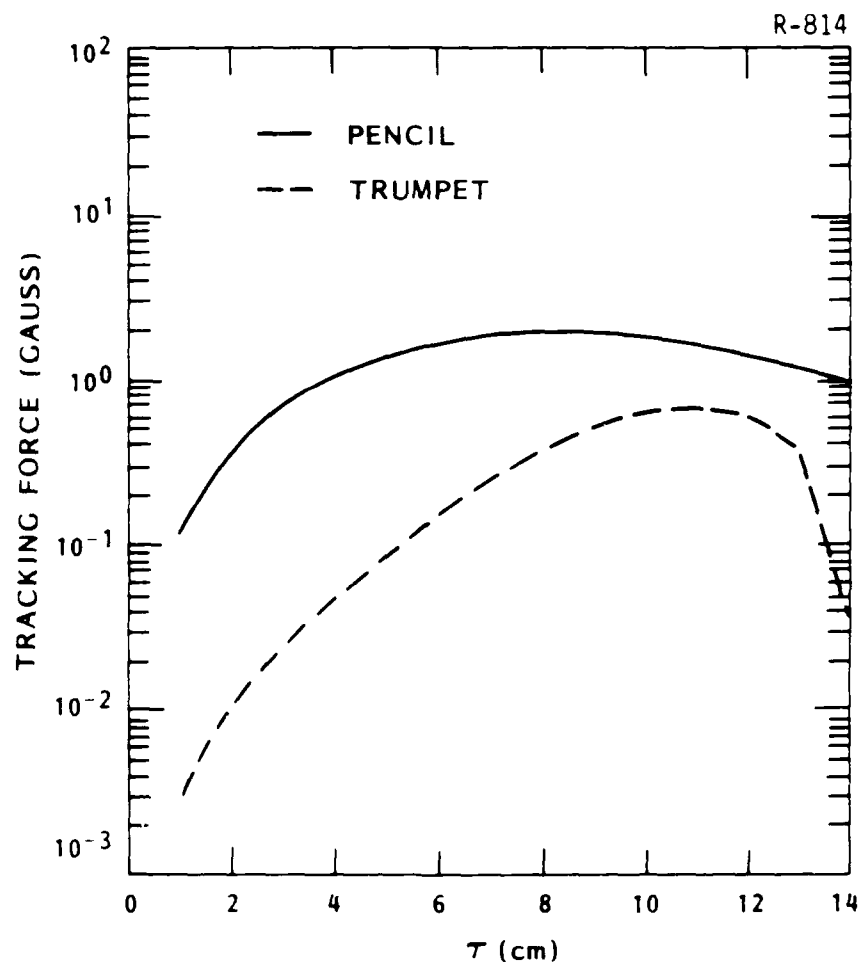


Figure 9. The tracking behavior of a trumpet beam and a 2-cm radius pencil beam is compared. The 3-cm conductivity channel was offset 0.75 cm. The trumpet beam is given by Eq. 33.

Since its effective radius is much greater, the trumpet beam needs a correspondingly greater channel radius to cause significant tracking. In Table 4, the optimal σ_0 and tracking force are listed for $r_c = 1$ to 8 cm. For the same r_c used in the pencil case (1 cm), the tracking force is negligible. However, a peak force of 0.78 gauss is computed for $r_c = 4$ cm. As before, the optimal σ_0 declines with increasing r_c indicative of magnetic detracking effects.

The results for trumpet beams in density and combination channels show slightly lower tracking than the conductivity channel except at large displacements as seen in the pencil beam case. Since the effective Bennett radius is much greater in the trumpet case, in a density channel, detracking effects are felt for larger displacements. The optimal displacement is correspondingly larger at 5 cm in a 3-cm radius channel. For this offset, the maximum tracking force is calculated at 5.6 gauss in the density channel (see Figure 10) and 4.8 gauss in the combination channel. In the density channel, the magnetic and electric components of the tracking force cancel until $\tau = 10$ cm. Beyond this point, the magnetic forces dominate until the electric component finally becomes tracking at $\tau = 18$ cm.

TABLE 4. TRUMPET BEAM TRACKING IN CONDUCTIVITY CHANNEL.

r_c (cm)	Optimal σ_0 (cm^{-1})	Maximum Tracking Force (gauss)
1	8.0	7×10^{-5}
2	2.8	0.052
3	1.2	0.51
4	0.78	0.78
8	0.70	0.70

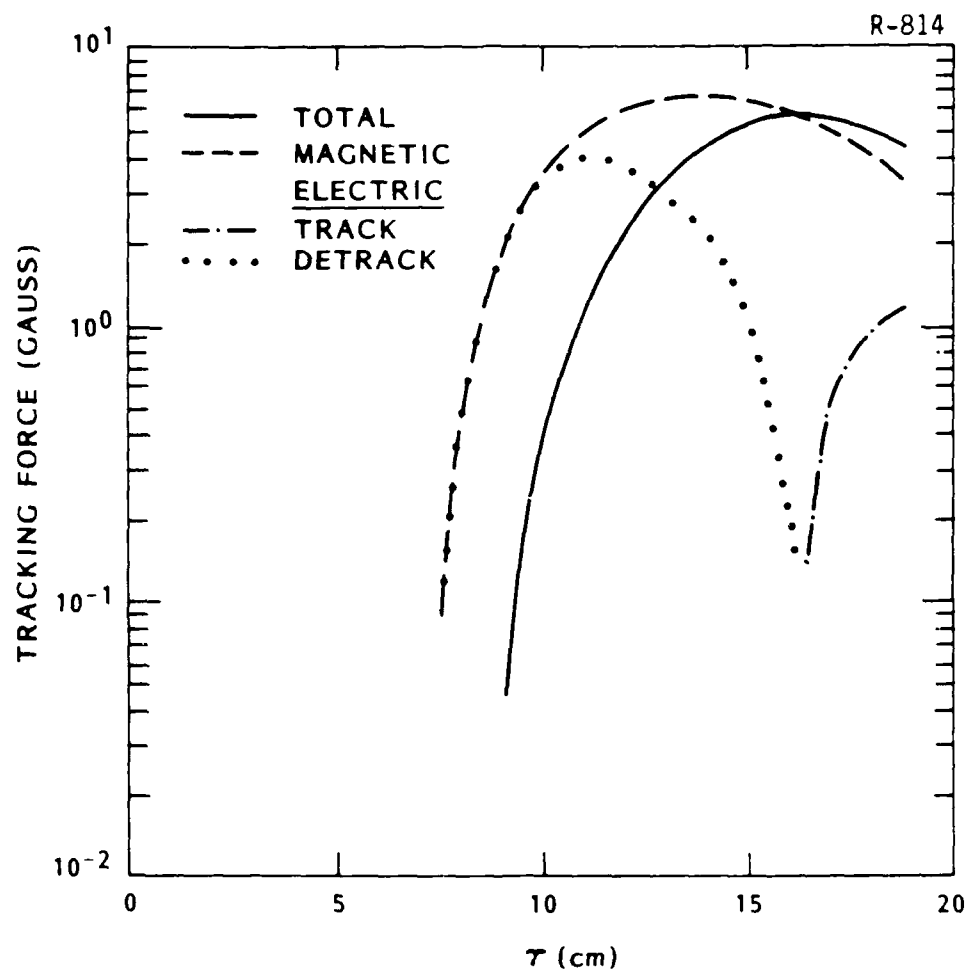


Figure 10. The tracking forces for a trumpet beam in a density channel is plotted. The 3-cm radius channel had a 0.1-atm on-axis density.

As seen in Figure 10, a trumpet beam experiences tracking well into the beam for large displacements ($\approx 1.5 r_c$). For all three types of channels, no net detracking was calculated up to $\tau = 20$ cm. This behavior is not nearly as pronounced in the pencil simulations. Since the beam-generated conductivity is more diluted in the trumpet-beam case, detracking axial return currents do not grow as fast. This effect is greatest at large displacements since the initial conductivity (avalanche-induced σ in the density channel case) near the beam is small.

CHAPTER 4

DISCUSSION

Analytic models and IPROP simulations have given us insight into the physical mechanisms of channel tracking. Electrostatic tracking is a secondary effect in a beam with short rise times (<4 ns) and $\sigma_0 < 5 \text{ cm}^{-1}$. This was seen to be true particularly in the case of a density channel, where electrostatic forces are generally detracking. Although the magnetic tracking must overcome the electric detracking, we still calculate very high forces on the order of 25 gauss for nominal parameters. When the more physically realistic trumpet beams were considered, 6-gauss tracking forces were still attainable at large displacements.

The magnetic component of the tracking force is driven by J_r and J_θ channel currents and by the dipole axial displacement current. The tracking currents are produced by the growing transverse electric fields. These currents in turn drive magnetic fields which attract the beam to the channel. The dipole axial displacement current is caused by the beam seeing an increasingly asymmetric channel-electron profile as τ increases for $\tau < 1/\sigma$. After a fast initial rise near the beam head, these fields decay roughly as $\exp(-\sigma\tau)$, as predicted in the analytic model.

The main parameter which determines whether a beam will track in either a conductivity or density channel is the amount of volume-integrated conductivity in the channel. This is evident from the lower optimal σ_0 calculated for larger radii channels. This conductivity coupled with the changing beam electric field produces a J_z channel return current. This oppositely flowing current will attempt to detrack an off-center beam. For beam-weighted σ above $1\text{-}2 \text{ cm}^{-1}$ in the nominal case, both the analytic expression and IPROP predict magnetic detracking.

The detracking axial return currents grow as σ builds up in the channel. This current growth is the result of the initial conductivity and

impact ionization of the beam. Close to the beam head, $E_z^{(0)}$ couples with the asymmetric conductivity that was present initially or produced via electron avalanche (in density channel) to produce dipole axial return currents. Also, the beam-generated conductivity couples with $E_z^{(1)}$. The detracking force produced at a radius r from the beam (r^+ is the point towards the channel axis and r^- is away from the channel) grows as,

$$F_{dt}(r) \approx (\sigma^+ - \sigma^-)E_z^{(0)}(r) + 2\sigma_1 E_z^{(1)}(r) \quad (34)$$

where σ_1 is the beam-symmetric conductivity produced in impact ionization at r from the beam axis. σ^+ and σ^- are the asymmetric conductivity at r^+ and r^- , respectively. For small τ , $E_z^{(0)}$ scales with $dI_z/d\tau$ and $E_z^{(1)}$ scales with $\sigma_0 dI_z/d\tau$. Since the magnitude of the asymmetric conductivity, with a correction for beam and channel radii, roughly determines $(\sigma^+ - \sigma^-)$, both terms in Eq. 34 increase with increasing σ_0 . We therefore expect smaller- σ_0 channels and longer rise time beams (σ_1 grows slower) to track longer.

As seen in Tables 1-3, there is a strong increase in the tracking force as the beam radius declines for a given beam current. This a_b dependence is caused by a greater fraction of the beam propagating in the channel for the smaller beam radius. Initially, a thin beam experiences enhanced magnetic tracking due to the large localized electric fields. However, for a given σ_0 , this beam will be repulsed sooner, since σ_1 will grow quickly close to the beam axis. For this reason, smaller- σ_0 channels are optimal for smaller- a_b beams. Since a greater percentage of the current lies in the channel where it is useful for tracking, a thin beam in a channel with small σ_0 experiences maximum channel tracking.

The trumpet-shaped beams behave similarly to the pencil beam, if we consider the beam to have a larger effective radius. The trumpet beam therefore requires a larger channel radius for good tracking. In the case we considered with an effective radius of 2 cm, the ideal channel had

$r_c = 4$ cm. This is similar to the scaling of the pencil beam which has a 1.2 cm ideal channel with $a_b = 0.5$ cm. This effect does tend to lower the maximum tracking due to the r_c^{-2} scaling of the tracking force.

CHAPTER 5

CONCLUSIONS

Maxwell's complete equations have yielded very optimistic estimates for channel tracking. Both analytic and numerical results show that the large magnitude of the tracking is the result of the magnetic forces produced near the beam head. These forces rise quickly before the electrostatic forces have had a chance to build up. The main detracking force, occurring at roughly $z = 5$ cm for the nominal beam/channel parameters, is also magnetic, resulting from channel return currents. The tracking force is as high as 6 gauss for a trumpet beam and up to 50 gauss for a pencil beam.

The effect of most beam/channel parameters, in the IPROP studies, is similar to that predicted in the analytic model derived in Section 2. The peak tracking force scales as $\epsilon I_0 \beta / r_c^2$ for $a_b, \epsilon \leq r_c$ in a Gaussian channel with initial conductivity. The tracking forces seen in IPROP simulations are severely degraded for $a_b \geq r_c$, with maximum tracking occurs for $\epsilon = a_b + r_c$. In the density and combination channels, the asymmetric conductivity produced through electron avalanche causes detracking for small ϵ ($< r_c/2$). However, for larger ϵ , the tracking force scales similarly to the conductivity channel.

Because of the large transverse dipole magnetic fields, a larger initial channel conductivity produces optimal tracking than previously thought. For a pencil beam in a 1-cm radius channel, the maximum tracking occurs with $\sigma_0 = 4.7 \text{ cm}^{-1}$, an order of magnitude higher than the 0.2 value suggested by Hui and Lampe⁷. The optimal conductivity declines with increasing channel radius, since channel return currents can occur in a larger volume, causing detracking. The optimal conductivity, therefore, scales as $1/r_c^2$.

In general, a trumpet beam behaves as a pencil beam with a larger effective radius. The maximum tracking is achieved in a correspondingly larger channel giving roughly an order of magnitude less force than a 0.5-cm radius pencil beam. One significant deviation from pencil behavior is the longer duration of the force in a trumpet beam. Because the small current density near the beam head produces a diluted beam-generated conductivity, the tracking force persists farther back into the trumpet beam particularly for $\epsilon \geq r_c$.

The results presented here are preliminary, since they were calculated assuming a slug beam. In this case, the tracking forces were easy to distinguish. In a dynamic beam, oscillations, particularly from the hose instability, can obscure these forces. In the near future, we will consider the more physical representation of an electron beam using IPROP with dynamic particles and hopefully better estimate the tracking force. The work presented in this paper does suggest we will find significantly higher forces than previously expected.

REFERENCES

1. E. P. Lee, "Calculation of a Tracking Force," UCID-19674, 1983.
2. B. B. Godfrey, "The IPROP Three-Dimensional Beam Propagation Code," Mission Research Report AMRC-R-690, 1985.
3. F. W. Chambers, "Mathematical Models for the Ringbearer Simulation Code," UCID-18302 (Lawrence Livermore Laboratory, 1979).
4. E. R. Parkinson and D. A. Keeley, "Studies in High Current Beam Propagation at Reduced Pressures," Science Applications International Corporation Report SAIC-C-U-75-PA, 1985.
5. E. P. Lee, "The New Field Equations," UCID-17286, 1976.
6. J. A. Masamitsu, S. S. Yu and F. W. Chambers, "Beam Tracking Studies with Ringbearer II," UCID-19771, 1982.
7. B. Hui and M. Lampe, "Numerical and Analytical Studies of Beam Channel Tracking," NRL Memorandum Report 5136, 1984.
8. B. Hui, private communication, March, 1986.
9. B. B. Godfrey, in Proc. Tenth Conf. Numerical Simulation of Plasmas, paper 1C6 (San Diego, 1983).

END

DATE

FILMED

5-88

DTIC